Exploring the Computational Design of Anionic Spin-Crossover Systems

*Laia Navarro[1] and Jordi Cirera[1]**

[1] Departament de Química Inorgànica i Orgànica and Institut de Recerca de Química Teòrica i Computacional, Universitat de Barcelona, Diagonal 645, 08028 Barcelona, Spain

e-mail: jordi.cirera@qi.ub.es

Abstract

In this work, a systematic study on how the ligand design in the anionic spin-crossover system $[Fe(OEt\text{-}L_1\text{-}pH)(NCS)_3]^-$ can be used to achieve a high degree of tuning on its transition temperature ($T_{1/2}$) is presented. Our calculations correctly reproduce the experimentally reported data, but allow us to gain further and systematic insight on how to tune up or down the $T_{1/2}$ value. The axial thiocyanate ligand can be replaced by similar groups (NCO^-, $NCSe^-$ and $NCBH_3^-$) that allows for a large change in the $T_{1/2}$, while a much finer degree of tuning can be achieved by functionalizing the *para* position of the pyridine groups. Altogether, the $[Fe(OEt\text{-}L_1\text{-}pH)(NCS)_3]^-$ offers a unique platform to explore how ligand design can be harvested to prepare new anionic SCO materials with tailored properties.

Keywords: Spin-Crossover, Transition Temperature, Coordination Compounds, Ligand-Field

1. Introduction

Switchable or stimuli responsive materials[1] are currently an active research area due to their potential technological applications in sensors,[2–4] molecular machines,[5] nanodevices,[6] energy storage[7,8] and self-healing materials,[8] among others. Among such type of materials, Spin-Crossover (SCO) systems,[9–14] which can switch reversibly between two alternative electronic states close in energy, are quite appealing systems due to their intrinsic behavior as molecular level switches.[15–18] This transition, which can be triggered by changing the temperature, but also with pressure or electromagnetic radiation,[19,20] comes with remarkable changes in the physical properties of the system, such as changes in the magnetic moment, the color, or structural distortions.[21,22] For all of the above, many SCO systems have been characterized over the last century. The phenomena was originally reported by Cambi in 1931 for Fe(III) coordination compounds,[23] but this field rapidly growth and expand to other transition metals,[24] and eventually expanded also to systems with higher nuclearity[25–27] and even coordination polymers which exhibit SCO transitions and are sensitive to the nature of their guest molecules.[28–31]

The field of SCO is vastly dominated by six coordinated Fe(II) compounds,[32–35] in which the transition is often induced by controlling the external temperature. The temperature with equal populations of both spin-states is defined as the transition temperature ($T_{1/2}$) and is a key parameter for the physical characterization of SCO systems,[36] but also a key value in terms of making such systems operational, because in principle, one might like to preselect the temperature at which the SCO transition occurs. This is, however, a quite challenging task from the experimental point of view. Even though major progress has been done in the field, understanding how to modulate the transition temperature using ligand design is a major deal in the rational design of new SCO systems with tailored properties. Because of this intrinsic problem, the use of computational tools has helped in gaining insight into how to modulate the

transition temperature in SCO systems, using a broad range of electronic structure methods at different levels of theory as well as machine learning protocols.[37–44]

Most SCO systems are either neutral or positively charged, but very few of them have been reported with a neat negative charge.[45–62] The lack of more anionic SCO systems is somehow problematic because such systems are key components in the design of fluorescent multifunctional materials and conducting switchable materials. Thus, the synthesis of new anionic SCO systems with tailored properties an important target towards the rational design of multifunctional materials that can operate at specific temperatures.[18,63] For that reason, we decided to study in detail the anionic SCO system $[Fe(OEt\text{-}L_1\text{-}pH)(NCS)_3]^-$ (L_1 = tris(pyridin-2-yl)ethoxymethane),[54] which allows for an important degree of chemical functionalization in the molecular skeleton, aiming to study the impact of such changes in the spin-state energy gap of the system, the corresponding transition temperatures, and the overall spin-crossover behavior of such systems. In this paper, we investigate the effect that three different possible sites in which chemical functionalization can be applied have over the $T_{1/2}$ in the family of the $[Fe(R_1\text{-}L_1\text{-}pH)(L_2)_3]^-$ (R_1 = O-R or CH_2-R, with R = H, -Me, -Et, -nPr and nBu, R_2 = $-NH_2$, -OH, -OMe, -Me, -F, -H, -Cl, -Br, $-CF_3$ and $-NO_2$, and L_2 = NCO^-, NCS^-, $NCSe^-$ and $NCBH_3^-$) anionic SCO systems. First, we will present the results from our computational studies, which will be later discussed in terms of the electronic structure for the analyzed systems. Finally, conclusions and outlook will be reported.

2. Computational Details

All density functional calculations (DFT) have been carried out with Gaussian 16 (revision B0.1)[64] electronic structure package with a 10^{-8} convergence criterion for the density matrix elements, using the latest triple-ζ basis set with polarization functions for all elements (def2-TZVP).[65] For all systems, the exchange correlation functional TPSSh has been used, which has

been recently reported as the most accurate one towards transition metal ions d^4-d^7 in terms of the spin-state energy gaps.[66] However, the calculation of spin-state energy gaps using Density Functional methods is a quite challenging problem.[67–70] Therefore, a benchmark on the $[Fe(OEt\text{-}L_1\text{-}pH)(NCS)_3]^-$ system was done, showing that only the TPSSh and OPBE[71,72] among several exchange/correlation functionals provide with the correct spin-state energy gap (see ESI). Finally, the TPSSh functional,[73] a hybrid version of the TPSS[74] meta-GGA functional with a 10% of exact exchange Hartree-Fock, was chosen due to its overall performance towards SCO systems. The corresponding vibrational analysis was done for all optimized structures to ensure that they were global minimums along the potential energy surface. The transition temperatures ($T_{1/2}$) were estimated using the thermochemistry quantities obtained in the vibrational analysis. To study the d-MOs energy gap in the low-spin systems (S=0), *n*-electron valence perturbation theory (NEVPT2)[75] calculations were performed using the Orca 4.0 computer code.[76] In these calculations, we employed the def2TZVPP basis set, including the corresponding auxiliary basis set for the correlation and Coulomb fitting. The active space contains the 5 d-orbitals of the metal and 4 electrons, and the *ab initio* ligand-field theory (AILFT) approach was employed to extract the related orbitals.[77]

3. Results

As indicated above, few anionic spin-crossover systems have been reported in the literature.[45–62] Among them, the Fe(II) compound $[Fe(OEt\text{-}L_1\text{-}pH)(NCS)_3]^-$ (L_1 = tris(pyridin-2-yl)ethoxymethane) offers us the possibility of studying how different chemical modifications on the ligand can be harvested to modify the physical properties of the compound allowing for, in principle, a fine degree of tuning on the $T_{1/2}$.[54] In Figure 1, we show the molecular structure of the parent compound, and a schematic depiction of the system with the three sites in which chemical modifications can be applied in order to alter the ligand field around the metal center,

and thus its SCO properties. Such sites are the R_1 group (ethoxy in the original system), the R_2 group, which is the *para* position of the pyridine groups (a H atom in the parent molecule), and finally the L_2 ligand, which is a NCS^- group in the original molecule. Therefore, one can systematically study the effect of modifying such sites over the spin-state energy gap in the system. Overall, the system of study can be labelled with the generic formula $[Fe(R_1\text{-}L_1\text{-}pR_2)(L_2)_3]^-$, which denotes the three positions in which we will apply chemical modifications to the molecule.

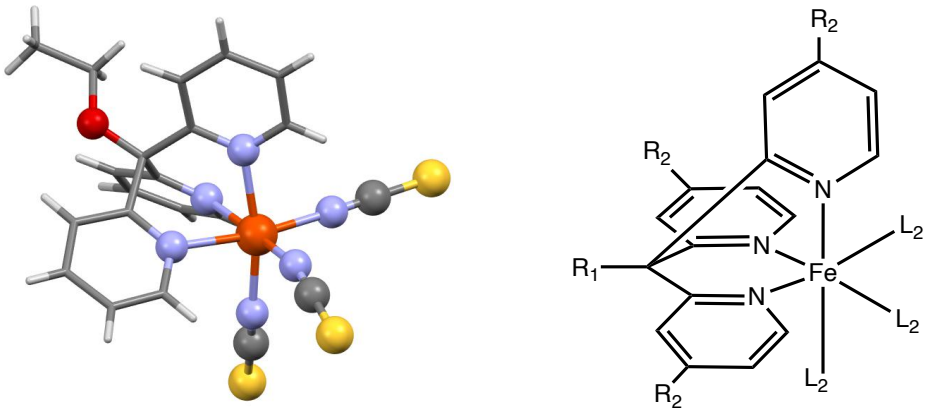

Figure 1: Left, the $[Fe(OEt\text{-}L_1\text{-}pH)(NCS)_3]^-$ (OEt-L_1-pH = tris(pyridin-2-yl)ethoxymethane) molecule.[54] Right, a schematic draw of the system of study indicating the different functionalization sites.

First, we studied the effect of replacing the thiocyanate (NCS^-) ligand by similar ligands, such as the selenocyanate and cyanoborohydride ligands ($NCSe^-$ and $NCBH_3^-$), which are stronger ligand field substituents than the original NCS^-, but we also tested the isocyanide ligand (NCO^-), a weaker one, to get a broader picture of the effect that L_2 has over the SCO properties of the $[Fe(OEt\text{-}L_1\text{-}pH)(L_2)_3]^-$ system. Results are summarized in Table 1.

$[Fe(OEt\text{-}L_1\text{-}pH)(L_2)_3]^-$	***ΔE***	***ΔH***	***ΔS***	$T_{1/2}$
$L_2 = NCS^-$	6.94	5.59	24.67	226 (170[a])
$L_2 = NCSe^-$	8.32	6.92	24.63	281
$L_2 = NCBH_3^-$	12.28	10.78	24.45	441 (313[a])
$L_2 = NCO^-$	1.73	0.49	20.70	24

Table 1: Computed ΔE, ΔH, ΔS and $T_{1/2}$ for the $[Fe(OEt\text{-}L_1\text{-}pH)(L_2)_3]^-$ systems. Electronic Energies and Enthalpies in kcal·mol^{-1}. Entropies in cal·K^{-1}·mol^{-1} and all temperatures in K. Experimental values (when available) in parenthesis. [a] Average value of reported $T_{1/2}$ (see ESI).

From the above, one can see that the experimentally reported trends for the $[Fe(OEt\text{-}L_1\text{-}pH)(NCS)_3]^-$ and $[Fe(OEt\text{-}L_1\text{-}pH)(NCBH_3)_3]^-$ are properly reproduced (see ESI),[53] with a similar shift in the computed $T_{1/2}$ as has been observed for previous calculations in SCO systems using the TPSSh functional.[37,66]

Next, we modified the R_1 group while keeping R_2 = H and $L_2 = NCS^-$. Two sets of substituents have been studied. First, alkane groups, starting from the smallest one (R_1 = H) and up to the *n*-butyl group. Secondly, alkoxide groups, starting from R_1 = OH and up to the n-butoxy group. Results are summarized in Table 2.

$[Fe(R_1\text{-}L_1\text{-}pH)(NCS)_3]^-$	***ΔE***	***ΔH***	***ΔS***	$T_{1/2}$
R_1 = H	8.32	7.02	23.82	295
R_1 = Me	10.48	9.15	23.50	389 (290)

R_1 = Et	6.97	5.63	24.66	228 (338)
R_1 = nPr	9.22	7.83	22.01	356 (298)
R_1 = nBu	9.34	7.97	23.84	334 (315)
R_1 = OH	9.03	7.70	23.32	330 (132)
R_1 = OMe	7.92	6.59	26.47	249 (245)
R_1 = OEt	6.94	5.59	24.67	226 (170[a])
R_1 = OnPr	9.42	8.00	23.15	346
R_1 = OnBu	7.12	5.75	24.39	236

Table 2: Computed ΔE, ΔH, ΔS and $T_{1/2}$ for the $[Fe(R_1\text{-}L_1\text{-}pH)(NCS)_3]^-$ systems. Electronic Energies and Enthalpies in kcal·mol^{-1}. Entropies in cal·K^{-1}·mol^{-1} and all temperatures in K. Experimental values in parenthesis. Experimental values (when available) in parenthesis. [a] Average value of reported $T_{1/2}$.

At this point, we did some control calculations to evaluate if the inclusion of the counterions was required. From table S2 in the ESI, it is possible to find a family of systems that have been characterized with three different counterions. The $[Fe(Me\text{-}L_1\text{-}pH)(NCS)_3]^-$ system has been studied using $[NMe_4]^+$, $[NBu_4]^+$ and $[PPh_4]^+$ as counterions. The experimental $T_{1/2}$ for such systems (313, 330 and 290 K respectively) seems to indicate that the impact of the counterion is minor, but we computed the corresponding $[Fe(Me\text{-}L_1\text{-}pH)(NCS)_3][C]$ systems (C =$[NMe_4]^+$, $[NBu_4]^+$ or $[PPh_4]^+$) to evaluate the impact of adding the counterion in the calculations. Once the spin-state energy gap was corrected for the basis set superposition error, the computed values are quite similar across the whole series, and slightly higher than the computed value for the anionic species (see S7 in ESI), indicating that the effect of the counterion is minimal. To further evaluate if the counterions were affecting the predicted

trends, we also computed the whole series for the [Fe(Me-L_1-pH)(L_2)$_3$][NMe_4] (L_2 = NCO^-, NCS^-, $NCSe^-$ and $NCBH_3^-$), and compared the trend with the one computed for the anionic families of [Fe(Me-L_1-pH)(L_2)$_3$]$^-$ and [Fe(OEt-L_1-pH)(L_2)$_3$]$^-$ systems (see S7 on the ESI). These results show that the critical difference between both systems arises from replacing a Me group by and OEt group in the R_1 position of the ligand, which has a much larger effect than doing the calculations with counterions. In fact, the experimentally reported shift for the $T_{1/2}$ between [Fe(Me-L_1-pH)(NCS)$_3$][NMe_4] ($T_{1/2}$ = 135 K) and [Fe(Me-L_1-pH)(NCS)$_3$][NMe_4] ($T_{1/2}$ = 313K) is 178 K, a quite close value as the one computed for the [Fe(Me-L_1-pH)(L_2)$_3$]$^-$ and [Fe(OEt-L_1-pH)(L_2)$_3$]$^-$ anionic systems (163 K), thus reinforcing the idea that the calculations grasp the nature of the changes in the ligand field strength around the Fe(II) metal center. More importantly, in all cases the computed with or without cations is the same.

Finally, we studied the effect that the *para*-substitution of the pyridine groups has over the SCO properties in the [Fe(OEt-L_1-pR_2)(L_2)$_3$]$^-$ systems. Here, we have been able to play with two chemical functionalizations at the same time. For each L_2 ligand, we studied several *p*-groups (R_2 = -NH_2, -OH, -OMe, -Me, -F, -H, -Cl, -Br, -CF_3 and -NO_2), covering from electron withdrawing groups (EWG) to electron donating groups (EDG). Results are summarized in Table 3, and the whole set of thermochemical data can be found in the ESI.

$[Fe(OEt\text{-}L_1\text{-}pR_2)(NCX)_3]^-$	***NCS⁻***		***NCSe⁻***		***$NCBH_3^-$***	
	ΔE	***$T_{1/2}$***	***ΔE***	***$T_{1/2}$***	***ΔE***	***$T_{1/2}$***
$R_2 = NH_2$	2.26	21	5.02	180	9.95	343
$R_2 = OH$	5.19	143	6.72	211	10.37	367
$R_2 = OMe$	5.30	167	6.85	221	10.67	381
$R_2 = Me$	6.51	200	7.92	251	11.87	515
$R_2 = F$	5.37	157	6.79	213	10.97	378
$R_2 = H$	6.94	226	8.32	281	12.28	441
$R_2 = Cl$	6.41	197	7.76	247	11.96	405
$R_2 = Br$	6.51	201	7.86	250	12.09	411
$R_2 = CF_3$	7.61	251	8.89	294	13.26	458
$R_2 = NO_2$	6.37	229	8.50	309	14.53	504

Table 3: Computed ΔE and $T_{1/2}$ for the $[Fe(OEt\text{-}L_1\text{-}pR_2)(L_2)_3]^-$ systems ($L_2 = NCS^-$, $NCSe^-$, and $NCBH_3^-$, and R_2 = -NH_2, -OH, -OMe, -Me, -F, -H, -Cl, -Br, -CF_3 and -NO_2). Electronic Energies and Enthalpies in kcal·mol^{-1}. Entropy in cal·K^{-1}·mol^{-1}. All Temperatures in K.

4. Discussion

As can be seen from above, significant changes in the SCO properties can be observed upon the chemical modifications applied to the $[Fe(R_1\text{-}L_1\text{-}pR_2)(L_2)_3]^-$ system. In the following section, we will discuss the origin of such changes and its trends, and the effect that such changes have over the ligand field splitting of the metal center.

To begin with, the length of the R_1 (R_1 = O-R or CH_2-R, R = -H, -Me, -Et, -*n*Pr and -*n*Bu) $[Fe(R_1\text{-}L_1\text{-}pH)(NCS)_3]^-$ system could be envisioned as a potential first place for tuning of the SCO properties in such molecules. However, asides from the fact that O-donor and C-donor

substituents have a different effect on the $T_{1/2}$, being the C-donor the ones that lead to higher $T_{1/2}$, the value of the transition temperature seems to be, at least from the electronic point of view, mostly independent of the length of the R chain. This can be observed in Figure 2, in which can be seen that the dependence of $T_{1/2}$ with the number of C atoms in the side chain becomes independent from each other. The O-donor groups tend to a stable value of 235 K, while the C-donor groups lead to a larger $T_{1/2}$ value of 356 K. So, even though different behaviors are observed between C-donor and O-donor, no dependence with the length of the -R group for the R_1 substituent can be outlined. These results are consistent with experimental studies on how the side chain in alkane/alkanoic side chains affect $T_{1/2}$.[78] We must stress at this point that although no significant electronic effects are observed, the length of this side chain (particularly for long chains) can play an important role in the crystal packing, thus modulating the overall shape of the spin-transition, but from the electronic point of view, the length of the side chain seems to have a minimal impact on the SCO properties of the $[Fe(R_1\text{-}L_1\text{-}pR_2)(L_2)_3]^-$ systems.

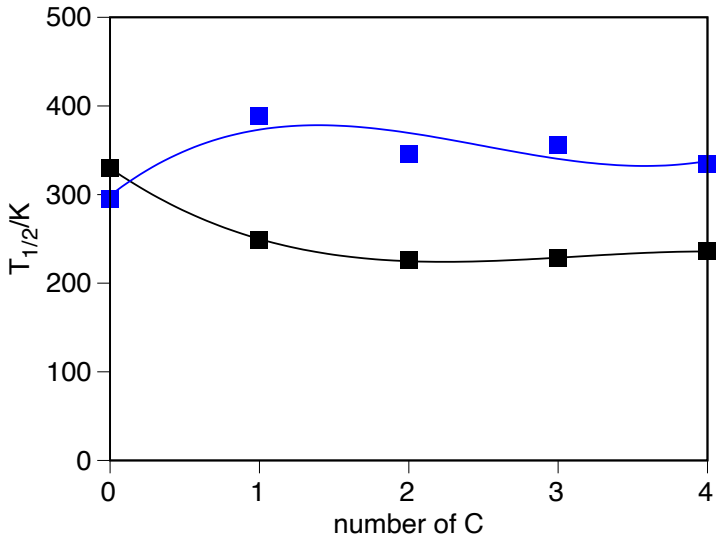

Figure 2: Computed $T_{1/2}$ for the $[Fe(R_1\text{-}L_1\text{-}pH)(NCS)_3]^-$ systems against the number of carbon atoms in the side chain of the R_1 group. Black, R_1 = O-R, and blue, R_1 = CH_2-R, while R = -H, -Me, -Et, -*n*Pr and -*n*Bu).

On the other hand, it is clear that changing L_2 in the $[Fe(OEt\text{-}L_1\text{-}pH)(L_2)_3]^-$ systems will have a major impact in the ligand field splitting of the Fe^{II} metal center. The increasing ligand strength, $NCO^- < NCS^- < NCSe^- < NCBH_3^-$, appears clearly reflected in the progressive shift in the computed $T_{1/2}$, as has been observed experimentally for some of these systems.[53] A nice correlation between the ligand *f* factor,[79] which measures the ligand strength, and the computed $T_{1/2}$ can be outlined, as seen in Figure 3. The magnitude of the d-MOs splitting can be properly quantified by using the *Ab Initio* Ligand Field Theory (AILFT) method to analyze the output from NEVPT2 calculations on the optimized geometries for all $[Fe(OEt\text{-}L_1\text{-}pH)(L_2)_3]^-$ low-spin systems. The computed Δ against the ligand *f* factor also reflects the increasing gap among the d-based MOs (see ESI), from 17200 to 18200 cm^{-1} between the weakest (NCO^-) and the strongest ($NCBH_3^-$) ligand. As it has been reported for similar systems, the increasing gap is due to the loss of partial antibonding character among the t_{2g} orbitals. These set of orbitals, which is non-bonding for the perfect octahedron with six σ-donor ligands, gains antibonding character due to the presence of π-type orbitals from the NCX^- ligands that can interact in π-antibonding fashion with the d_{xz}, d_{yz} and d_{xy} orbitals. However, as the L_2 ligand becomes stronger, these π-type orbitals move down in energy, thus effectively decreasing the interaction the d-MOs, that regain non-bonding character, and thus lead to larger Δ values. In Figure 4, we plotted the HOMO for the $[Fe(OEt\text{-}L_1\text{-}pH)(L_2)_3]^-$ systems (L_2 = NCO^-, NCS^-, $NCSe^-$ and $NCBH_3^-$) to illustrate such effect.

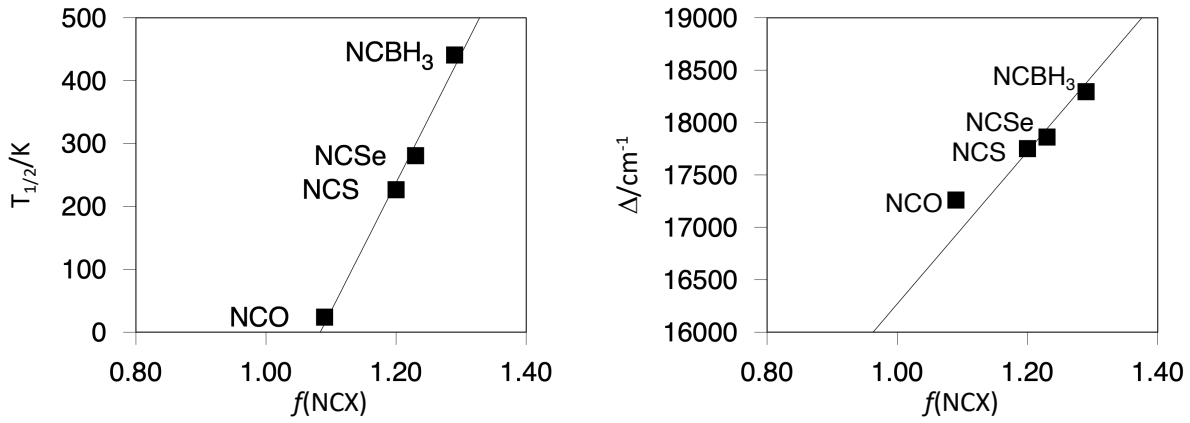

Figure 3: Correlation between the ligand *f* factor and the computed $T_{1/2}$ (left), and the computed Δ (right).

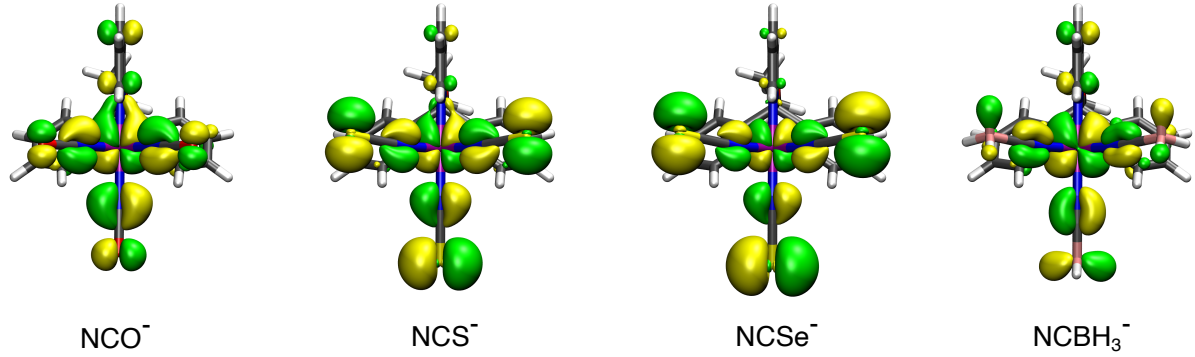

Figure 4: Isosurfaces for the HOMO d-based MOs on the $[Fe(OEt\text{-}L_1\text{-}pH)(L_2)_3]^-$ systems (L_2 = NCO^-, NCS^-, $NCSe^-$ and $NCBH_3^-$) (0.03 $au^{-3/2}$ isovalue contour).

Another way of tuning the $T_{1/2}$, in a more subtle way, is by using electron donor (EDG) or electron withdrawing (EWG) groups as substituents in the *para* position of the pyridine ring. This effect has been already reported in other SCO systems, and shows $T_{1/2}$ shifts towards higher values as the EDG character of the *para*-substituent increases. We decided to study how such substitutions impacts the SCO properties, and functionalized the pyridine group of the OEt-L_1-*p*R_2 ligand (R_2 = -NH_2, -OH, -OMe, -Me, -F, -H, -Cl, -Br, -CF_3 and -NO_2) in the $[Fe(OEt\text{-}L_1\text{-}pR_2)(NCS)_3]^-$ system. As expected, EWG lead to smaller values of the $T_{1/2}$, and this parameter can be tuned up by replacing the R_2 group with a more EDG substituent. In fact,

a correlation with the Hammett σ_p+ parameter[80] (or the σ_p constant, see ESI) can be outlined (Figure 5), in agreement with this behavior, as has been previously observed for other SCO systems.[81–87] This trend thus allows for a fine tuning degree of the $T_{1/2}$ for the [Fe(OEt-L_1-*p*R_2)$(NCS)_3$]$^-$ system, and we decided to explore if a similar behavior would occur for the other [Fe(OEt-L_1-*p*R_2)$(L_2)_3$]$^-$ systems. Our results show that, actually, a very similar degree of fine tuning is observed regardless the L_2 ligand (L_2 = NCS^-, $NCSe^-$, and $NCBH_3^-$), meaning that one can select a specific range of temperatures by using L_2, and later on select a much finer degree of tuning of $T_{1/2}$ via the R_2 substituent of the pyridine ligands. A similar trend is also observed for the NCO^-, but the weaker nature of this ligand makes that in the majority of cases, the system becomes a high-spin system, and only the most EDG have an impact in increasing $T_{1/2}$ (see ESI).

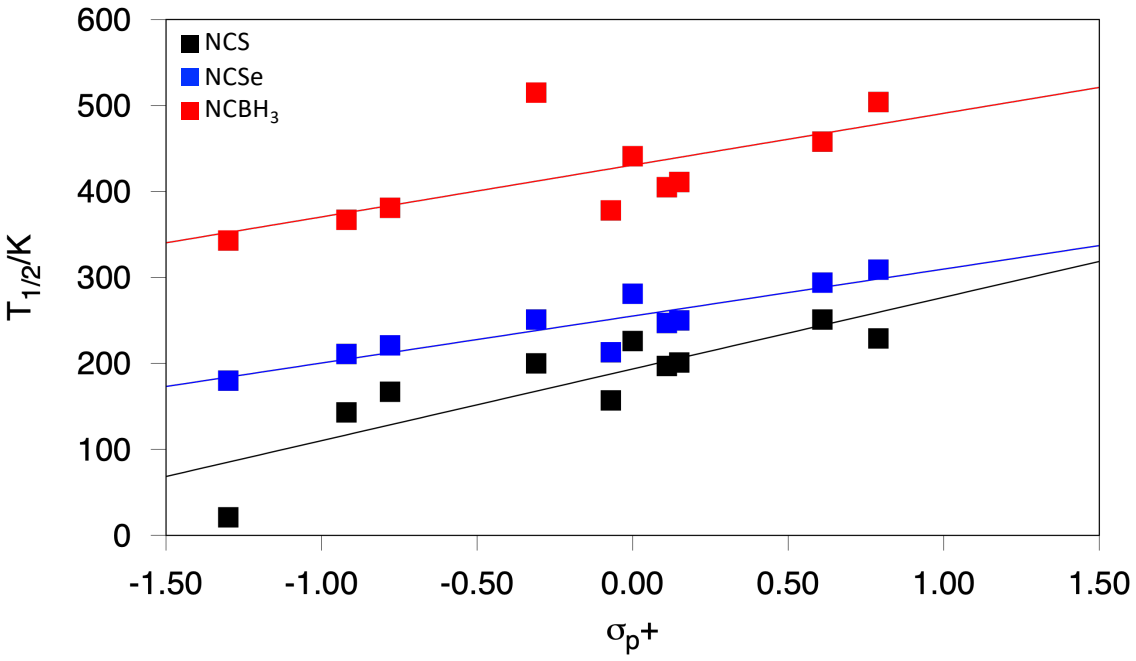

Figure 5: Computed $T_{1/2}$ vs. the σ_p+ Hammett parameter for the [Fe(OEt-L_1-*p*R_2)$(L_2)_3$]$^-$ systems. L_2 are in black (NCS^-), blue ($NCSe^-$) and red ($NCBH_3^-$), and R_2 = $-NH_2$, -OH, -OMe, -Me, -F, -H, -Cl, -Br, $-CF_3$ and $-NO_2$.

5. Conclusions

In this work, the TPSSh functional has been used to analyze the SCO properties of the $[Fe(OEt\text{-}L_1\text{-}pH)(NCS)_3]^-$ system, one of the few anionic SCO molecules reported in the literature. In order to expand this family of compounds and design systems with specific physical properties, we used our computational methodology to study the effect that different functionalizations will have over the spin-state energy gap for different members of the $[Fe(R_1\text{-}L_1\text{-}pR_2)(L_2)_3]^-$ family, in which several chemical modifications over the basic molecular structure have been studied. Functionalization of the R_1 does lead to some differences, but the length of the aliphatic chain seems to play a minor role on the modulation of the $T_{1/2}$. In any case, the role of this side chain cannot be overlooked in terms of modifying the SCO properties through crystal packing effects. On the other hand, by changing the L_2 ligands one can access a broad range of transition temperatures, that can later be fine-tuned using the R_2 groups of the pyridine ligand. Our results show that a two-knob model can be outlined, in which one can select a higher or lower $T_{1/2}$ value by using different L_2 ligands, and achieve a much precise value on such quantity through the pyridine functionalization in the para position. All trends can be understood in terms of the electronic structure of the studied systems, and several correlations have been outlined that predict the changes that $T_{1/2}$ will experience upon ligand modification. We believe that our results will be of great help in the future design of new anionic SCO systems that will operate at specific transition temperatures.

Author information:

jordi.cirera@qi.ub.es

Notes: The authors declare no competing financial interest.

Acknowledgments:

J.C. thanks the Spanish MICINN for a Ramón y Cajal research contract (RYC2018-024692-I), the Spanish MICINN research grant (PID2020-115165GB-I00) and the Spanish Structures of Excellence María de Maeztu program (MDM-2017-0767). L. N. is grateful for a PREDOCS-UB 2019 grant (5760700-Institut de Química Teòrica i Computacional).

References:

(1) Urban, M. W. *Handbook of Stimuli-Responsive Materials*; Urban, M. W., Ed.; Wiley, 2011. https://doi.org/10.1002/9783527633739.

(2) Qin, P.; Okur, S.; Li, C.; Chandresh, A.; Mutruc, D.; Hecht, S.; Heinke, L. A Photoprogrammable Electronic Nose with Switchable Selectivity for VOCs Using MOF Films. *Chem. Sci.* **2021**. https://doi.org/10.1039/d1sc05249g.

(3) Ohba, M.; Yoneda, K.; Agustí, G.; Muñoz, M. C.; Gaspar, A. B.; Real, J. A.; Yamasaki, M.; Ando, H.; Nakao, Y.; Sakaki, S.; Kitagawa, S. Bidirectional Chemo-Switching of Spin State in a Microporous Framework. *Angew. Chemie Int. Ed.* **2009**, *48* (26), 4767–4771. https://doi.org/10.1002/anie.200806039.

(4) Darabi, A.; Jessop, P. G.; Cunningham, M. F. CO 2 -Responsive Polymeric Materials: Synthesis, Self-Assembly, and Functional Applications. *Chem. Soc. Rev.* **2016**, *45* (15), 4391–4436. https://doi.org/10.1039/C5CS00873E.

(5) Aprahamian, I. The Future of Molecular Machines. *ACS Cent. Sci.* **2020**, *6* (3), 347–358. https://doi.org/10.1021/acscentsci.0c00064.

(6) Natelson, D. *Nanostructures and Nanotechnology*; Cambridge University Press, 2015. https://doi.org/10.1017/CBO9781139025485.

(7) Sun, C.; Wang, C.; Boulatov, R. Applications of Photoswitches in the Storage of Solar Energy. *ChemPhotoChem* **2019**, *3* (6), 268–283. https://doi.org/10.1002/cptc.201900030.

(8) Goulet-Hanssens, A.; Eisenreich, F.; Hecht, S. Enlightening Materials with Photoswitches. *Adv. Mater.* **2020**, *32* (20), 1905966. https://doi.org/10.1002/adma.201905966.

(9) Halcrow, M. A. *Spin-Crossover Materials*; HALCROW, M. A., Ed.; John Wiley & Sons Ltd: Oxford, UK, 2013. https://doi.org/10.1002/9781118519301.

(10) Molnár, G.; Rat, S.; Salmon, L.; Nicolazzi, W.; Bousseksou, A. Spin Crossover Nanomaterials: From Fundamental Concepts to Devices. *Adv. Mater.* **2018**, *30* (5), 1703862. https://doi.org/10.1002/adma.201703862.

(11) Gütlich, P. Spin Crossover - Quo Vadis? *Eur. J. Inorg. Chem.* **2013**, *2013* (5–6), 581–591. https://doi.org/10.1002/ejic.201300092.

(12) Gütlich, P.; Goodwin, H. A. *Spin Crossover in Transition Metal Compounds III*; Topics in Current Chemistry; Springer Berlin Heidelberg: Berlin, Heidelberg, 2004; Vol. 235. https://doi.org/10.1007/b96439.

(13) Senthil Kumar, K.; Ruben, M. Emerging Trends in Spin Crossover (SCO) Based Functional Materials and Devices. *Coord. Chem. Rev.* **2017**, *346*, 176–205. https://doi.org/10.1016/j.ccr.2017.03.024.

(14) Gütlich, P.; Gaspar, A. B.; Garcia, Y. Spin State Switching in Iron Coordination Compounds. *Beilstein J. Org. Chem.* **2013**, *9*, 342–391. https://doi.org/10.3762/bjoc.9.39.

(15) Muñoz, M. C.; Real, J. A. Thermo-, Piezo-, Photo- and Chemo-Switchable Spin

Crossover Iron(II)-Metallocyanate Based Coordination Polymers. *Coord. Chem. Rev.* **2011**, *255* (17–18), 2068–2093. https://doi.org/10.1016/j.ccr.2011.02.004.

(16) Halcrow, M. A. Structure:Function Relationships in Molecular Spin-Crossover Complexes. *Chem. Soc. Rev.* **2011**, *40* (7), 4119. https://doi.org/10.1039/c1cs15046d.

(17) Boldog, I.; Gaspar, A. B.; Martínez, V.; Pardo-Ibañez, P.; Ksenofontov, V.; Bhattacharjee, A.; Gütlich, P.; Real, J. A. Spin-Crossover Nanocrystals with Magnetic, Optical, and Structural Bistability near Room Temperature. *Angew. Chemie - Int. Ed.* **2008**, *47* (34), 6433–6437. https://doi.org/10.1002/anie.200801673.

(18) Benaicha, B.; Van Do, K.; Yangui, A.; Pittala, N.; Lusson, A.; Sy, M.; Bouchez, G.; Fourati, H.; Gómez-García, C. J.; Triki, S.; Boukheddaden, K. Interplay between Spin-Crossover and Luminescence in a Multifunctional Single Crystal Iron(II) Complex: Towards a New Generation of Molecular Sensors. *Chem. Sci.* **2019**, *10* (28), 6791–6798. https://doi.org/10.1039/C9SC02331C.

(19) Gütlich, P.; Gaspar, A. B.; Garcia, Y.; Ksenofontov, V. Pressure Effect Studies in Molecular Magnetism. *Comptes Rendus Chim.* **2007**, *10* (1–2), 21–36. https://doi.org/10.1016/j.crci.2006.09.011.

(20) Real, J. A.; Gaspar, A. B.; Muñoz, M. C. Thermal, Pressure and Light Switchable Spin-Crossover Materials. *Dalton Trans.* **2005**, No. 12, 2062. https://doi.org/10.1039/b501491c.

(21) Alvarez, S. Relationships between Temperature, Magnetic Moment, and Continuous Symmetry Measures in Spin Crossover Complexes. *J. Am. Chem. Soc.* **2003**. https://doi.org/10.1021/ja0283450.

(22) Oppermann, M.; Zinna, F.; Lacour, J.; Chergui, M. Chiral Control of Spin-Crossover Dynamics in Fe(II) Complexes. *Nat. Chem.* **2022**, *14* (7), 739–745. https://doi.org/10.1038/s41557-022-00933-0.

(23) Cambi, L.; Szegö, L. Über Die Magnetische Susceptibilität Der Komplexen Verbindungen. *Berichte der Dtsch. Chem. Gesellschaft (A B Ser.* **1931**, *64* (10), 2591–2598. https://doi.org/10.1002/cber.19310641002.

(24) Olguín, J. Unusual Metal Centres/Coordination Spheres in Spin Crossover Compounds. *Coord. Chem. Rev.* **2020**, *407* (15), 213148. https://doi.org/10.1016/j.ccr.2019.213148.

(25) Murray, K. S. Advances in Polynuclear Iron(II), Iron(III) and Cobalt(II) Spin-Crossover Compounds. *Eur. J. Inorg. Chem.* **2008**, *2008* (20), 3101–3121. https://doi.org/10.1002/ejic.200800352.

(26) Hogue, R. W.; Singh, S.; Brooker, S. Spin Crossover in Discrete Polynuclear Iron(II) Complexes. *Chem. Soc. Rev.* **2018**, *47* (19), 7303–7338. https://doi.org/10.1039/C7CS00835J.

(27) Breuning, E.; Ruben, M.; Lehn, J.-M.; Renz, F.; Garcia, Y.; Ksenofontov, V.; Gütlich, P.; Wegelius, E.; Rissanen, K. Spin Crossover in a Supramolecular Fe4II [2×2] Grid Triggered by Temperature, Pressure, and Light. *Angew. Chemie Int. Ed.* **2000**, *39* (14), 2504–2507. https://doi.org/10.1002/1521-3773(20000717)39:14<2504::AID-ANIE2504>3.0.CO;2-B.

(28) Zhu, X.-W.; Luo, D.; Zhou, X.-P.; Li, D. Imidazole-Based Metal-Organic Cages: Synthesis, Structures, and Functions. *Coord. Chem. Rev.* **2022**, *455*, 214354. https://doi.org/10.1016/j.ccr.2021.214354.

(29) Li, H.-Y.; Zhao, S.-N.; Zang, S.-Q.; Li, J. Functional Metal–Organic Frameworks as Effective Sensors of Gases and Volatile Compounds. *Chem. Soc. Rev.* **2020**, *49* (17), 6364–6401. https://doi.org/10.1039/C9CS00778D.

(30) Nakaya, M.; Ohtani, R.; Hayami, S. Guest Modulated Spin States of Metal Complex Assemblies. *Eur. J. Inorg. Chem.* **2020**, *2020* (39), 3709–3719.

https://doi.org/10.1002/ejic.202000553.

(31) Bartual-Murgui, C.; Akou, A.; Thibault, C.; Molnár, G.; Vieu, C.; Salmon, L.; Bousseksou, A. Spin-Crossover Metal–Organic Frameworks: Promising Materials for Designing Gas Sensors. *J. Mater. Chem. C* **2015**, *3* (6), 1277–1285. https://doi.org/10.1039/C4TC02441A.

(32) Chuang, Y.-C.; Liu, C.-T.; Sheu, C.-F.; Ho, W.-L.; Lee, G.-H.; Wang, C.-C.; Wang, Y. New Iron(II) Spin Crossover Coordination Polymers $[Fe(\mu\text{-}Atrz)_3]X_2 \cdot 2H_2O$ (X = $ClO4^-$, $BF4^-$) and $[Fe(\mu\text{-}Atrz)(\mu\text{-}Pyz)(NCS)_2]\cdot 4H_2O$ with an Interesting Solvent Effect. *Inorg. Chem.* **2012**, *51* (8), 4663–4671. https://doi.org/10.1021/ic202626c.

(33) Ashley, D. C.; Jakubikova, E. Ironing out the Photochemical and Spin-Crossover Behavior of Fe(II) Coordination Compounds with Computational Chemistry. *Coord. Chem. Rev.* **2017**, *337*, 97–111. https://doi.org/10.1016/j.ccr.2017.02.005.

(34) Scott, H. S.; Staniland, R. W.; Kruger, P. E. Spin Crossover in Homoleptic Fe(II) Imidazolylimine Complexes. *Coord. Chem. Rev.* **2018**, *362*, 24–43. https://doi.org/10.1016/j.ccr.2018.02.001.

(35) Gütlich, P.; Garcia, Y.; Goodwin, H. A. Spin Crossover Phenomena in Fe(Ii) Complexes. *Chem. Soc. Rev.* **2000**, *29* (6), 419–427. https://doi.org/10.1039/b003504l.

(36) Kahn, O. *Molecular Magnetism*; VCH, 1993.

(37) Cirera, J.; Paesani, F. Theoretical Prediction of Spin-Crossover Temperatures in Ligand-Driven Light-Induced Spin Change Systems. *Inorg. Chem.* **2012**, *51* (15), 8194–8201. https://doi.org/10.1021/ic300750c.

(38) Cirera, J.; Ruiz, E. Theoretical Modeling of the Ligand-Tuning Effect over the Transition Temperature in Four-Coordinated Fe-II Molecules. *Inorg. Chem.* **2016**, *55* (4), 1657–1663. https://doi.org/10.1021/acs.inorgchem.5b02564.

(39) Rudavskyi, A.; Sousa, C.; de Graaf, C.; Havenith, R. W. A.; Broer, R. Computational

Approach to the Study of Thermal Spin Crossover Phenomena. *J. Chem. Phys.* **2014**, *140* (18), 184318. https://doi.org/10.1063/1.4875695.

(40) Vela, S.; Fumanal, M.; Cirera, J.; Ribas-Arino, J. Thermal Spin Crossover in FeII and FeIII. Accurate Spin State Energetics at the Solid State. *Phys. Chem. Chem. Phys.* **2020**, *22* (9), 4938–4945. https://doi.org/10.1039/D0CP00162G.

(41) Cirera, J.; Ruiz, E. Computational Modeling of Transition Temperatures in Spin-Crossover Systems. *Comments Inorg. Chem.* **2019**, *39* (4), 216–241. https://doi.org/10.1080/02603594.2019.1608967.

(42) Janet, J. P.; Chan, L.; Kulik, H. J. Accelerating Chemical Discovery with Machine Learning: Simulated Evolution of Spin Crossover Complexes with an Artificial Neural Network. *J. Phys. Chem. Lett.* **2018**, *9* (5), 1064–1071. https://doi.org/10.1021/acs.jpclett.8b00170.

(43) Navarro, L.; Rodriguez, F.; Cirera, J. Controlling the Spin-Crossover Behavior of the [Cr(Indenyl) 2] Family via Ligand Functionalization. *Dalton Trans.* **2021**, *50* (25), 8704–8710. https://doi.org/10.1039/D1DT00481F.

(44) Vidal, D.; Cirera, J.; Ribas-Arino, J. Accurate Calculation of Spin-State Energy Gaps in Fe(III) Spin-Crossover Systems Using Density Functional Methods. *Dalton Trans.* **2021**, *50* (47), 17635–17642. https://doi.org/10.1039/D1DT03335B.

(45) Phonsri, W.; Lewis, B. A. I.; Jameson, G. N. L.; Murray, K. S. Double Spin Crossovers: A New Double Salt Strategy to Improve Magnetic and Memory Properties. *Chem. Commun.* **2019**, *55* (93), 14031–14034. https://doi.org/10.1039/C9CC07416C.

(46) Phonsri, W.; Macedo, D. S.; Lewis, B. A. I.; Wain, D. F.; Murray, K. S. Iron(III) Azadiphenolate Compounds in a New Family of Spin Crossover Iron(II)–Iron(III) Mixed-Valent Complexes. *Magnetochemistry* **2019**, *5* (2), 37.

https://doi.org/10.3390/magnetochemistry5020037.

(47) Gómez, V.; Sáenz de Pipaón, C.; Maldonado-Illescas, P.; Waerenborgh, J. C.; Martin, E.; Benet-Buchholz, J.; Galán-Mascarós, J. R. Easy Excited-State Trapping and Record High T_{TIESST} in a Spin-Crossover Polyanionic Fe^{II} Trimer. *J. Am. Chem. Soc.* **2015**, *137* (37), 11924–11927. https://doi.org/10.1021/jacs.5b07879.

(48) Hirosawa, N.; Oso, Y.; Ishida, T. Spin Crossover and Light-Induced Excited Spin-State Trapping Observed for an Iron(II) Complex Chelated with Tripodal Tetrakis(2-Pyridyl)Methane. *Chem. Lett.* **2012**, *41* (7), 716–718. https://doi.org/10.1246/cl.2012.716.

(49) Yamasaki, M.; Ishida, T. Spin-Crossover Thermal Hysteresis and Light-Induced Effect on Iron(II) Complexes with Tripodal Tris(2-Pyridyl)Methanol. *Polyhedron* **2015**, *85*, 795–799. https://doi.org/10.1016/j.poly.2014.10.013.

(50) Yamasaki, M.; Ishida, T. Heating-Rate Dependence of Spin-Crossover Hysteresis Observed in an Iron(II) Complex Having Tris(2-Pyridyl)Methanol. *J. Mater. Chem. C* **2015**, *3* (30), 7784–7787. https://doi.org/10.1039/C5TC00926J.

(51) Ishida, T.; Kanetomo, T.; Yamasaki, M. An Iron(II) Complex Tripodally Chelated with 1,1,1-Tris(Pyridin-2-Yl)Ethane Showing Room-Temperature Spin-Crossover Behaviour. *Acta Crystallogr. Sect. C Struct. Chem.* **2016**, *72* (11), 797–801. https://doi.org/10.1107/S2053229616004174.

(52) Kashiro, A.; Some, K.; Kobayashi, Y.; Ishida, T. Iron(II) and 1,1,1-Tris(2-Pyridyl)Nonadecane Complex Showing an Order–Disorder-Type Structural Transition and Spin-Crossover Synchronized over Both Conformers. *Inorg. Chem.* **2019**, *58* (12), 7672–7676. https://doi.org/10.1021/acs.inorgchem.9b01146.

(53) Cuza, E.; Benmansour, S.; Cosquer, N.; Conan, F.; Pillet, S.; Gómez-García, C. J.; Triki, S. Spin Cross-Over (SCO) Anionic Fe(II) Complexes Based on the Tripodal

Ligand Tris(2-Pyridyl)Ethoxymethane. *Magnetochemistry* **2020**, *6* (2), 26. https://doi.org/10.3390/magnetochemistry6020026.

(54) Cuza, E.; Mekuimemba, C. D.; Cosquer, N.; Conan, F.; Pillet, S.; Chastanet, G.; Triki, S. Spin Crossover and High-Spin State in Fe(II) Anionic Polymorphs Based on Tripodal Ligands. *Inorg. Chem.* **2021**, *60* (9), 6536–6549. https://doi.org/10.1021/acs.inorgchem.1c00335.

(55) Murata, S.; Takahashi, K.; Sakurai, T.; Ohta, H.; Yamamoto, T.; Einaga, Y.; Shiota, Y.; Yoshizawa, K. The Role of Coulomb Interactions for Spin Crossover Behaviors and Crystal Structural Transformation in Novel Anionic Fe(III) Complexes from a π-Extended ONO Ligand. *Crystals* **2016**, *6* (5), 49. https://doi.org/10.3390/cryst6050049.

(56) Takahashi, K.; Kawamukai, K.; Okai, M.; Mochida, T.; Sakurai, T.; Ohta, H.; Yamamoto, T.; Einaga, Y.; Shiota, Y.; Yoshizawa, K. A New Family of Anionic Fe III Spin Crossover Complexes Featuring a Weak-Field N 2 O 4 Coordination Octahedron. *Chem. - A Eur. J.* **2016**, *22* (4), 1253–1257. https://doi.org/10.1002/chem.201504883.

(57) Cook, C.; Habib, F.; Aharen, T.; Clérac, R.; Hu, A.; Murugesu, M. High-Temperature Spin Crossover Behavior in a Nitrogen-Rich Fe III -Based System. *Inorg. Chem.* **2013**, *52* (4), 1825–1831. https://doi.org/10.1021/ic301864d.

(58) Li, Z.-Y.; Dai, J.-W.; Shiota, Y.; Yoshizawa, K.; Kanegawa, S.; Sato, O. Multi-Step Spin Crossover Accompanied by Symmetry Breaking in an Fe III Complex: Crystallographic Evidence and DFT Studies. *Chem. - A Eur. J.* **2013**, *19* (39), 12948–12952. https://doi.org/10.1002/chem.201302272.

(59) Floquet, S.; Guillou, N.; Négrier, P.; Rivière, E.; Boillot, M.-L. The Crystallographic Phase Transition for a Ferric Thiosemicarbazone Spin Crossover Complex Studied by X-Ray Powder Diffraction. *New J. Chem.* **2006**, *30* (11), 1621–1627. https://doi.org/10.1039/B605326B.

(60) Floquet, S.; Boillot, M.-L.; Rivière, E.; Varret, F.; Boukheddaden, K.; Morineau, D.; Négrier, P. Spin Transition with a Large Thermal Hysteresis near Room Temperature in a Water Solvate of an Iron(Iii) Thiosemicarbazone Complex. *New J. Chem.* **2003**, *27* (2), 341. https://doi.org/10.1039/b207516d.

(61) Karuppannan, S. K.; Martín-Rodríguez, A.; Ruiz, E.; Harding, P.; Harding, D. J.; Yu, X.; Tadich, A.; Cowie, B.; Qi, D.; Nijhuis, C. A. Room Temperature Conductance Switching in a Molecular Iron(III) Spin Crossover Junction. *Chem. Sci.* **2021**, *12* (7), 2381–2388. https://doi.org/10.1039/D0SC04555A.

(62) Yamada, M.; Ooidemizu, M.; Ikuta, Y.; Osa, S.; Matsumoto, N.; Iijima, S.; Kojima, M.; Dahan, F.; Tuchagues, J.-P. Interlayer Interaction of Two-Dimensional Layered Spin Crossover Complexes [FeIIH3LMe][FeIIL Me]X (X - = ClO_4- , BF_3- , PF_6- , AsF_6- , and SbF_6 - ; H3L. *Inorg. Chem.* **2003**, *42* (25), 8406–8416. https://doi.org/10.1021/ic034439e.

(63) Coronado, E.; Galán-Mascarós, J. R.; Gómez-García, C. J.; Laukhin, V. Coexistence of Ferromagnetism and Metallic Conductivity in a Molecule-Based Layered Compound. *Nature* **2000**, *408* (6811), 447–449. https://doi.org/10.1038/35044035.

(64) Frisch, M. J.; Trucks, G. W.; Schlegel, H. B.; Scuseria, G. E.; Robb, M. A.; Cheeseman, J. R.; Scalmani, G.; Barone, V.; Petersson, G. A.; Nakatsuji, H.; Li, X.; Caricato, M.; Marenich, A. V.; Bloino, J.; Janesko, B. G.; Gomperts, R.; Mennucci, B.; Hratchian, H. P.; Ortiz, J. V.; Izmaylov, A. F.; Sonnenberg, J. L.; Williams-Young, D.; Ding, F.; Lipparini, F.; Egidi, F.; Goings, J.; Peng, B.; Petrone, A.; Henderson, T.; Ranasinghe, D.; Zakrzewski, V. G.; Gao, J.; Rega, N.; Zheng, G.; Liang, W.; Hada, M.; Ehara, M.; Toyota, K.; Fukuda, R.; Hasegawa, J.; Ishida, M.; Nakajima, T.; Honda, Y.; Kitao, O.; Nakai, H.; Vreven, T.; Throssell, K.; Montgomery, J. A., J.; Peralta, J. E.; Ogliaro, F.; Bearpark, M. J.; Heyd, J. J.; Brothers, E. N.; Kudin, K. N.;

Staroverov, V. N.; Keith, T. A.; Kobayashi, R.; Normand, J.; Raghavachari, K.; Rendell, A. P.; Burant, J. C.; Iyengar, S. S.; Tomasi, J.; Cossi, M.; Millam, J. M.; Klene, M.; Adamo, C.; Cammi, R.; Ochterski, J. W.; Martin, R. L.; Morokuma, K.; Farkas, O.; Foresman, J. B.; Fox, D. J. Gaussian 16, Rev. B.01. *Gaussian, Inc., Wallingford, CT* **2016**.

(65) Weigend, F.; Ahlrichs, R. Balanced Basis Sets of Split Valence, Triple Zeta Valence and Quadruple Zeta Valence Quality for H to Rn: Design and Assessment of Accuracy. *Phys. Chem. Chem. Phys.* **2005**, *7* (18), 3297–3305. https://doi.org/10.1039/b508541a.

(66) Cirera, J.; Via-Nadal, M.; Ruiz, E. Benchmarking Density Functional Methods for Calculation of State Energies of First Row Spin-Crossover Molecules. *Inorg. Chem.* **2018**, *57* (22), 14097–14105. https://doi.org/10.1021/acs.inorgchem.8b01821.

(67) Swart, M. Accurate Spin-State Energies for Iron Complexes. *J. Chem. Theory Comput.* **2008**, *4* (12), 2057–2066. https://doi.org/10.1021/ct800277a.

(68) Swart, M. Spin States of (Bio)Inorganic Systems: Successes and Pitfalls. *Int. J. Quantum Chem.* **2013**, *113* (1), 2–7. https://doi.org/10.1002/qua.24255.

(69) Kepp, K. P. Theoretical Study of Spin Crossover in 30 Iron Complexes. *Inorg. Chem.* **2016**, *55* (6), 2717–2727. https://doi.org/10.1021/acs.inorgchem.5b02371.

(70) Jensen, K. P.; Cirera, J. Accurate Computed Enthalpies of Spin Crossover in Iron and Cobalt Complexes. *J. Phys. Chem. A* **2009**, *113* (37), 10033–10039. https://doi.org/10.1021/jp900654j.

(71) Handy, N. C.; Cohen, A. J. Left-Right Correlation Energy. *Mol. Phys.* **2001**, *99* (5), 403–412. https://doi.org/10.1080/00268970010018431.

(72) Perdew, J. P.; Burke, K.; Ernzerhof, M. Generalized Gradient Approximation Made Simple [Phys. Rev. Lett. 77, 3865 (1996)]. *Phys. Rev. Lett.* **1997**, *78* (7), 1396.

(73) Staroverov, V. N.; Scuseria, G. E.; Tao, J. M.; Perdew, J. P. Comparative Assessment of a New Nonempirical Density Functional: Molecules and Hydrogen-Bonded Complexes. *J. Chem. Phys.* **2003**, *119* (23), 12129–12137. https://doi.org/10.1063/1.1626543.

(74) Tao, J.; Perdew, J. P.; Staroverov, V. N.; Scuseria, G. E. Climbing the Density Functional Ladder: Nonempirical Meta–Generalized Gradient Approximation Designed for Molecules and Solids. *Phys. Rev. Lett.* **2003**, *91* (14), 146401. https://doi.org/10.1103/PhysRevLett.91.146401.

(75) Angeli, C.; Cimiraglia, R.; Malrieu, J. P. N-Electron Valence State Perturbation Theory: A Spinless Formulation and an Efficient Implementation of the Strongly Contracted and of the Partially Contracted Variants. *J. Chem. Phys.* **2002**, *117* (20), 9138–9153. https://doi.org/10.1063/1.1515317.

(76) Neese, F. Software Update: The ORCA Program System, Version 4.0. *WIREs Comput. Mol. Sci.* **2018**, *8* (1), e1327. https://doi.org/10.1002/wcms.1327.

(77) Singh, S. K.; Eng, J.; Atanasov, M.; Neese, F. Covalency and Chemical Bonding in Transition Metal Complexes: An Ab Initio Based Ligand Field Perspective. *Coord. Chem. Rev.* **2017**, *344*, 2–25. https://doi.org/10.1016/j.ccr.2017.03.018.

(78) Kashiro, A.; Kohno, W.; Ishida, T. Odd–Even Effect on the Spin-Crossover Temperature in Iron(II) Complex Series Involving an Alkylated or Acyloxylated Tripodal Ligand. *Inorg. Chem.* **2020**, *59* (14), 10163–10171. https://doi.org/10.1021/acs.inorgchem.0c01296.

(79) Jørgensen, C. K. *Modern Aspects of Ligand Field Theory*; North-Holland Publishing, Ed.; 1971.

(80) Hansch, C.; Leo, A.; Taft, R. W. A Survey of Hammett Substituent Constants and Resonance and Field Parameters. *Chem. Rev.* **1991**, *91* (2), 165–195.

https://doi.org/10.1021/cr00002a004.

(81) Tweedle, M. F.; Wilson, L. J. Variable Spin Iron(III) Chelates with Hexadentate Ligands Derived from Triethylenetetramine and Various Salicylaldehydes. Synthesis, Characterization, and Solution State Studies of a New 2T .Dblarw. 6A Spin Equilibrium System. *J. Am. Chem. Soc.* **1976**, *98* (16), 4824–4834. https://doi.org/10.1021/ja00432a023.

(82) Létard, J.-F.; Carbonera, C.; Real, J. A.; Kawata, S.; Kaizaki, S. Photomagnetism of a Series of Dinuclear Iron(II) Complexes. *Chem. - A Eur. J.* **2009**, *15* (16), 4146–4155. https://doi.org/10.1002/chem.200802171.

(83) Prat, I.; Company, A.; Corona, T.; Parella, T.; Ribas, X.; Costas, M. Assessing the Impact of Electronic and Steric Tuning of the Ligand in the Spin State and Catalytic Oxidation Ability of the Fe II (Pytacn) Family of Complexes. *Inorg. Chem.* **2013**, *52* (16), 9229–9244. https://doi.org/10.1021/ic4004033.

(84) Kershaw Cook, L. J.; Kulmaczewski, R.; Mohammed, R.; Dudley, S.; Barrett, S. A.; Little, M. A.; Deeth, R. J.; Halcrow, M. A. A Unified Treatment of the Relationship Between Ligand Substituents and Spin State in a Family of Iron(II) Complexes. *Angew. Chemie Int. Ed.* **2016**, *55* (13), 4327–4331. https://doi.org/10.1002/anie.201600165.

(85) Kimura, A.; Ishida, T. Pybox-Iron(II) Spin-Crossover Complexes with Substituent Effects from the 4-Position of the Pyridine Ring (Pybox = 2,6-Bis(Oxazolin-2-Yl)Pyridine). *Inorganics* **2017**, *5* (3), 52. https://doi.org/10.3390/inorganics5030052.

(86) Liang, H.-C.; Pan, Y.; Zhu, H.-L.; Meng, Y.-S.; Liu, C.-H.; Liu, T.; Zhu, Y.-Y. The Substituent Effect on the Spin-Crossover Behaviour in a Series of Mononuclear Fe(II) Complexes from Thio-Pybox Ligands. *Inorg. Chem. Front.* **2022**, *9* (10), 2343–2352. https://doi.org/10.1039/D2QI00208F.

(87) Kulmaczewski, R.; Howard, M. J.; Halcrow, M. A. Influence of Ligand Substituent Conformation on the Spin State of an Iron(II)Di(Pyrazol-1-Yl)Pyridine Complex. *Dalton Trans.* **2021**, *50* (10), 3464–3467. https://doi.org/10.1039/D1DT00590A.